REU Final Paper: Analysis and Improvement of a Six-Axis Robotic Scanner for Millimeter-Wave Active Phased Array Antenna Calibration

Robert Baines, Rodrigo Lebrón, and Jorge Salazar

Abstract— **Herein, a novel proof-of-concept experimental setup proposed by Dr. Salazar at the Radar Innovations Laboratory was constructed and optimized to assess the effects of temperature variations on phased array radar calibration. The system is fully automated and programmable with a graphical user interface and allows surface, thermal, and radio frequency characterization. The controllable hardware consists of an environmental chamber and a robot arm mounted with an infrared camera, high definition camera, laser, and radio frequency scanner that perform automated analysis of a chosen antenna under test. This paper, in addition to describing the experimental setup in detail, catalogues the analysis and amelioration of system parameters.**

I. INTRODUCTION

Phased array radar (PAR) is the next logical step in radar technology for both forecasting and military applications because it poses numerous advantages over conventional dish radar. Foremost, PAR enables faster scan times—even up an order of magnitude compared to widespread WSR-88D Doppler radars (Zrnic et al). Enhanced scan times allow forecasters to more accurately and promptly inform the public when severe weather is imminent. As the National Severe Storms Laboratory stated in a press release (2006, p.2), PAR "has the potential to increase the average lead time for tornado warnings well beyond the current average of 11 minutes." When severe weather can sporadically change, a difference of minutes can mean saved lives.

While PARs pose major benefits in the realm of forecasting, they are multifunctional instruments and can be employed simultaneously in military applications. The nature of their design enables multiple targets to be scanned at once by individually controllable beams from arrays on the PAR. For instance, PARs, while gathering meteorological information can be electronically directed to identify objects with radio frequency and guide missiles, or track entities across the entire sky. They can also be employed as communication devices between distant receivers and transmitters (Theodore and Frank).

Even though they are broadly applicable, PARs remain low profile, boasting light weight, conformability to desired geometry, and small-size compared to conventional dish radars (Theodore and Frank). In fact, PARs operate electronically and contain no moving mechanical parts, which extends their lifetime and decreases long-term maintenance costs. Whereas conventional dish radar can require up to $500,000 per month to maintain, PAR decreases this hefty sum to a manageable amount over time.
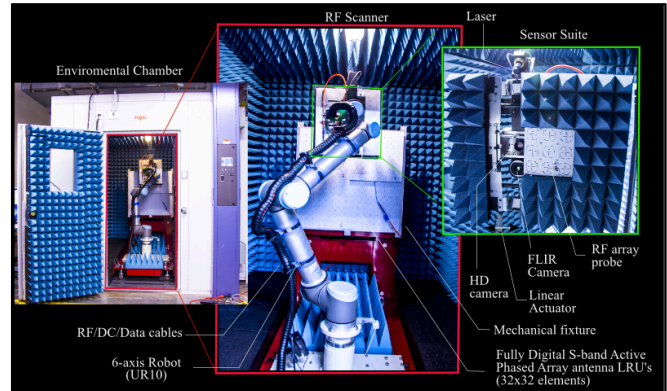

Figure 1. The six-axis robotic scanning system in environmental chamber

Despite their many merits, in order to be operational in real-life circumstances, PARs must be able to be calibrated in the environment in which they are deployed. Owing to their high functionality, PARs are found everywhere from military battleships to remote outposts. In environments such as these, temperature is a factor when considering PAR calibration. Namely, fluctuations in ambient temperature affect layers of the antenna stack of the phased array and consequently changes its broadcasting characteristics (Wang et al). Herein, a fully automated, novel experimental setup originally proposed by Dr. Salazar is described that allows for the assessment of temperature influence on PAR calibration.

The setup, as shown in Figure 1, consists of an environmental chamber outfitted with anechoic microwave-absorbing cones, wherein a six-degree of freedom (6DOF) robotic manipulator equipped with sensors can scan a given Antenna Under Test (AUT). Control of environmental parameters, robot trajectory, and sensor data is managed via an encompassing graphical user interface.

Ultimately, the automatic nature of the experimental setup allows for streamlined experiments and data acquisition of great relevance for compensation by calibration techniques. Information gathered from these experiments will enhance understanding of phased array radar performance in realistic conditions and pave the road to full-scale implementation.

Section two of this paper prefaces experimental description with theoretical calculations, showing how broadcasting characteristics of a PAR will distort under varying temperature conditions. Then, section three specifies system architecture and components. The fourth section discusses current performance, highlighting areas for improvement. Finally, the fifth section describes steps taken to ameliorate the setup.
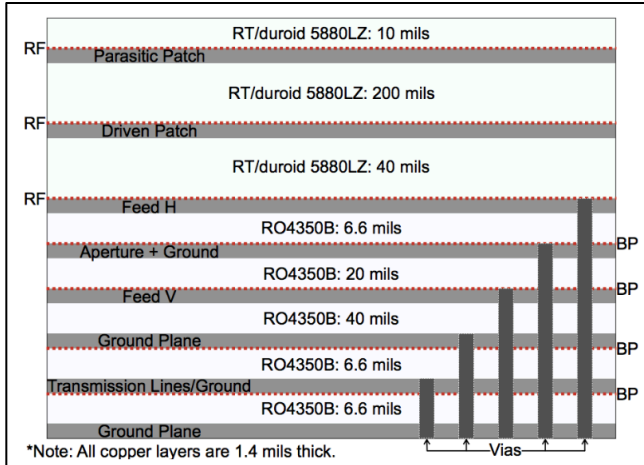
J. Salazar and R. Lebrón are with the Department of Electrical and Computer Engineering at the University of Oklahoma, Norman, OK, 73019, see http://www.arrc.ou.edu/. Robert Baines is a mechanical engineering student at Rice University at 6100 Main Street Houston, TX, 77005, and NWC REU participant. Email: rlb7@rice.edu

Chart 1. Material layers comprising the Horus Antenna Stack. This will eventually be tested in the automated characterization system.

II. THEORETICAL CALCULATIONS

The physical expansion of filaments in an antenna stack dictates phase distortions in the X, Y, and Z planes. These phase changes can be used to adapt perceived antenna calibration values to ones that reflect the environmental variability. I calculated the thermal expansion and consequent phase distortion of an antenna stack to be used in the chamber, the Horus antenna. These values provide a basis of comparison for future experimental values. The following equation gives the linear thermal expansion of a solid:

$$\Delta L = L * CTE * \Delta T \qquad (1)$$

where L is the length in a particular dimension, CTE is the coefficient of temperature expansion, and ΔT is the change in temperature experienced by the solid. Materials used in the antenna stack are presented in Chart 1.

The following equation gives the phase change in terms of expansion:

$$\Delta \phi = \frac{2\pi}{\lambda_g} * d \qquad (2)$$

where d is the change in x, y, or z, $\lambda_g = \frac{\lambda_0}{\sqrt{\varepsilon_{eff}}}$, and λ_0 = c/f , and ε_{eff} is a function of a number of material properties. Table 1 in the appendix expresses the calculated thermal expansions in X, Y, and Z directions for each filament, in addition to the predicted phase distortions. Calculated thermal expansion values and their corresponding phase distortions fall within an expected range.

III. SETUP

A. Environmental Chamber

An Espec brand environmental chamber was employed, and we outfitted it with ETS-Lindgren microwave absorbers for the 3 Ghz frequency to mitigate unwanted reflected electromagnetic waves. The ensuing radio-silent environment allows for undisturbed characterization of antennas. Although the chamber has the capacity to replicate environments from -50 to 90 C, for experimental purposes simulating realistic operating conditions, it will be used from -10 C to 50 C.
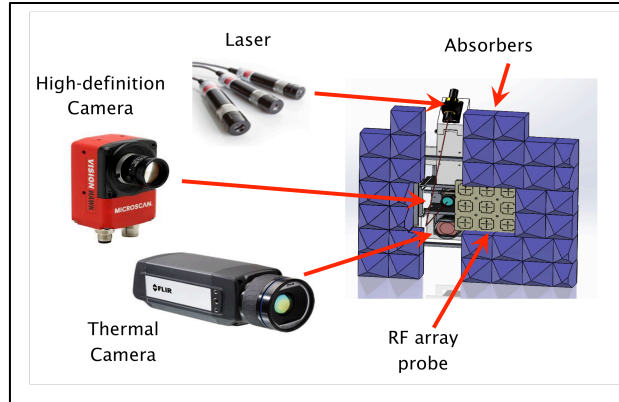

Figure 2. End effector payload equipped with sensors, laser, and absorbers. Opening and closing of the absorbers is controlled by a linear actuator.

B. Robotic Manipulator

We used a 6 degree-of-freedom Universal Robots UR10 manipulator to hold the radio frequency probe and various sensors for scanning the phased array antenna. Since it is 6DOF, the robot has the ability to move in the x, y, and z directions. As such, a chosen antenna under test is not constrained by any conventional planar geometry. The robot is advertised to have a repeatability of 100 micrometers.

C. Sensor Suite

The sensor suite consists of all sensors and the hardware required to support them, as illustrated in Figure 2. Sensors mounted on the robot end effector consist of a FLIR thermal camera for thermal characterization, a Microscan High-Definition camera for surface measurements, a custom Radio frequency (RF) scanner designed in-lab for radio frequency measurements, and a Coherence Stingray laser for tracking end effector position relative to the antenna surface. The sensor array comprises an additional linear actuator, such that a barrier of microwave absorbers can be closed and opened at will, allowing the RF probe to capture data without interference from onboard electronics or metallic surfaces from the sensor suite.

D. User Interface

The entire system including environmental control, robotic trajectory, and sensor data acquisition, is controlled via a master graphical user interface coded in LabView (Figure 3). The interface was designed to be intuitive, straightforward, and comprehensive. Accordingly, the program informs the user which step it is currently performing via a progress bar and an array of pilot lights.

Operation of the graphical user interface consists of three distinct steps. First, the user selects the desired elements on the array they wish to measure. Graphically, this is depicted by 4 quadrants of 8x8 buttons, each element on the array represented by the corresponding buttons within the quadrants. Second, temperature and humidity parameters are entered. The user has the option of up to 8 distinct temperature steps, each from -10 to 50 C, ramp or constant behavior, and time allotted to each step.
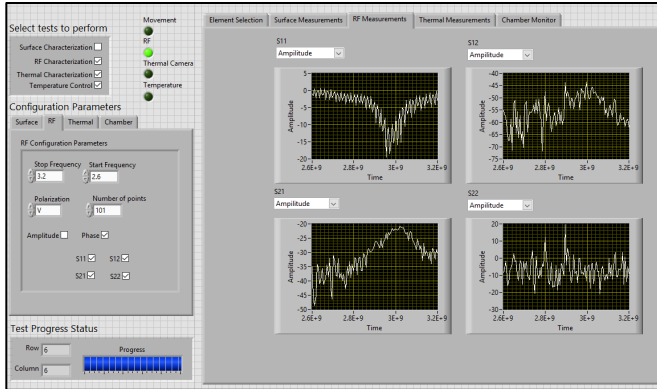
Figure 3. User interface featuring a test progress bar and tab control to various monitoring graphs

Figure 4. Points at which robot believed it was centered on the first element over 40 trials at 0 C.

Up to 20 distinct temperature sequences may be saved in the system and recalled automatically. Lastly, with a click of 'GO,' automated operation starts.

Data acquisition is automatically handled; users are presented a sequence of tabs that display RF measurements, thermal imaging, surface imaging, and a chamber temperature monitor. After a given test is performed, the program stores a log of all recorded data points and entered user parameters in a designated path on the operating system.

IV. CURRENT PERFORMANCE

A. Calibration of the Positioning System

In order to ensure accurate characterization of the antenna under test, the position and orientation of the robot must be ascertained. This process consists of 3 distinct steps. First, the robot's built-in kinematics provides a rough estimate of the location of its end effector. Second, an HD camera used in conjunction with machine vision identifies and precisely centers the sensor suite according to each array element's contours. The center point is demarked by a fiducial; the machine vision operates by delimiting distinct contours around a fiducial to pixel resolution. Third, the laser provides the relative distance of the end effector from the array surface at any time during operation.

To determine the efficacy and accuracy of the positioning mechanisms, we instructed the robot to travel to each element on the array up to 40 times. Namely, in a typical trial, the robot centered its HD camera where it perceived the center of an array element to be. Then it traveled to the subsequent adjacent element, again centering its HD camera at the alleged center. Upon arrival at the end of a row, the robot cycled back to the first fiducial again to repeat the entire series. In this fashion, we were able to determine the reproducibility of the robot trajectory. The experiment was conducted in varying temperature ranges to see if temperature influenced reproducibility.

Results are promising. Fig 4 displays the first element of the test; the complete panorama is in the appendix. Clearly, the robot stayed within a fair range of the goal 100 micrometer diameter (delimited by the solid circle). Mean error is delimited by the dashed circle. The trial indicates some irreproducibility, thoug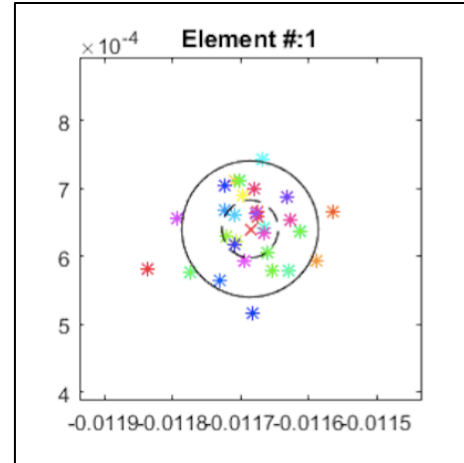h, as several points lie outside of goal range. We attribute the inaccuracy primarily to the weight of robot payload because it surpassed recommended capacity and induced discrete fluctuations in the actuators.

V. IMPROVEMENTS AND OPTIMIZATION

Attempting to correct the robot's instability, the aluminum robot payload was consecutively replaced with 3D printed parts. The extruded matrix of PLA Makerbot printed parts makes them significantly lighter and sufficiently robust for experimental purposes. In addition, PLA filament has a very low coefficient of thermal expansion in the -10 to 50 C temperature range, which precludes imaging error from hardware shift ("Quadrant - Global Manufacturer Of Engineering Plastics, High Performance Plastics, High Temperature Plastic Materials")

Using SolidWorks computer-aided design software, I created components to support and manage the wires running to and from the robot payload. The wire manager design had a number of iterations because the payload was gradually altered to accommodate more hardware. Initially, a simple holder was created (a); it was found, though, that the holder did not effectively constrain the wires when the robot moved in the horizontal direction. The second iteration (b) fixed this issue by incorporating a tapered well that secured the wires. However, the rearranging of a bolt in the payload architecture undermined the second design and necessitated space to allow the bolt head to protrude. Thus, the third iteration was created (c). A last minute alteration was made to the architecture of the wiring, so I printed the final working prototype, pictured in figure 6.
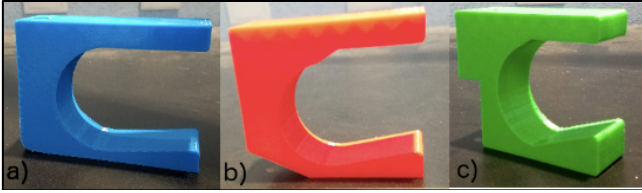
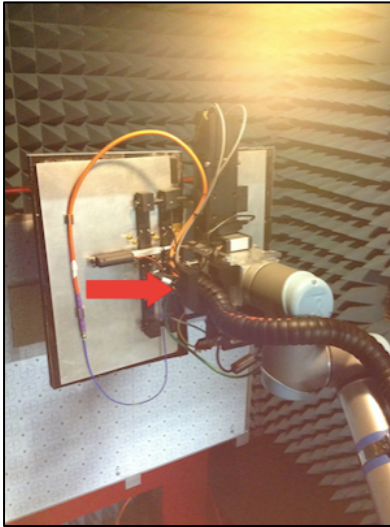Figure 5. Evolution of design: a) first concept, b) second, c) third

Figure 6. Final prototype wire manager in-use, effectively preventing wire interference with moving robot arm

Figure 7. CAD model of payload with sensors. Parts highlighted in cyan are to be replaced with the 3D printed components shown on the right.

As a second initiative, I created replacements for four parts of the supporting hardware of the robot payload, effectively lowering the weight by 2.7 lbs. We believe that this decrease in weight will have notable impact on the reproducibility of the robot trajectory. The CAD model and physical part are displayed in Figure 7. Helical inserts were employed to provide thread to screw fixtures, because 3D printed material is not conducive to threading. Another problem arose when conducting trial runs. Unfortunately, due to the thermal reflectivity of the antenna under test, the FLIR infrared camera actually picked up its own reflection in the captured image as it was trying to discern the array element. The effect was particularly pronounced when observed at colder temperatures, such as 0 C. As the chamber cooled, the electronics in the camera became increasingly vibrant compared to the chilled hardware and air around it; thus its thermal profile was accentuated. We addressed the issue of thermal reflectivity by changing the surface of the antenna under test to a less reflective material. Further plans have been devised to circumvent the thermal disturbance such as mounting the thermal camera at an angle and encasing much of its housing in glass since infrared cannot penetrate glass.

VI. CONCLUSION

In sum, an innovative experimental setup initially envisioned by Dr. Salazar was constructed and optimized to allow for full characterization of phased array antennas under varying temperature conditions. The system as it stands is 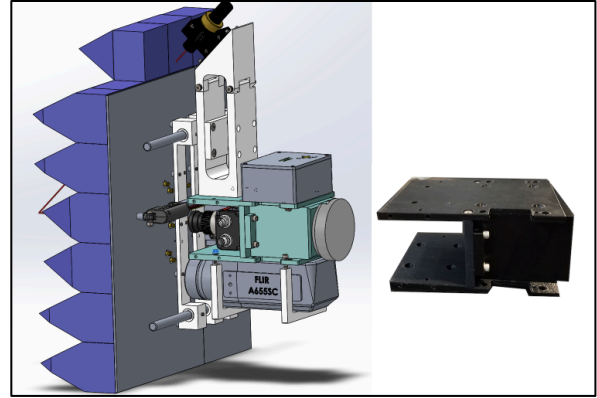operable but future efforts will continue to focus on ameliorating the reproducibility of the robot trajectory and machine vision recognition algorithms. This unique system will enhance the body of knowledge surrounding PAR performance and contribute to their full-scale implementation. As a summer intern in the Radar Innovations Laboratory, I personally assisted with the construction of the chamber, assembly of the robot, wire management, interfacing system controls, creating a graphical user interface to streamline experimental processes, calibration of electromagnetic measurement equipment, theoretical phase calculations, and replacing the payload with 3D printed parts.

APPENDIX

TABLE I

CALCULATED THERMAL EXPANSION AND PHASE DISTORTION HORUS ANTENNA AT 3 GHz AND 0-25 C

Layer	Thermal Expansion (x,y,z) [mm]	Phase Distortion (x,y,z) [degrees]
1	4.4704, 4.3688, 0.0026	17.0534, 16.6658, 0.0101
2	1.6967, 1.6967, 0.0001	6.4725, 6.4725, 0.0006
3	4.4704, 4.3688, 0.0527	17.0534, 16.6658, 0.2011
4	1.6967, 1.6967, 0.0001	6.4725, 6.4725, 0.0006
5	4.4704, 4.3688, 0.0105	17.0534, 16.6658, 0.0402
6	1.6967, 1.6967, 0.0001	6.4725, 6.4725, 0.0006
7	1.0160, 1.2192, 0.0013	3.8758, 4.6509, 0.0051
8	1.6967, 1.6967, 0.0001	6.4725, 6.4725, 0.0006
9	1.0160, 1.2192, 0.0041	3.8758, 4.6509, 0.0155
10	1.6967, 1.6967, 0.0001	6.4725, 6.4725, 0.0006
11	1.0160, 1.2192, 0.0081	3.8758, 4.6509, 0.0310
12	1.6967, 1.6967, 0.0001	6.4725, 6.4725, 0.0006
13	1.0160, 1.2192, 0.0013	3.8758, 4.6509, 0.0051
14	1.6967, 1.6967, 0.0001	6.4725, 6.4725, 0.0006
15	1.0160, 1.2192, 0.0013	3.8758, 4.6509, 0.0051
16	1.6967, 1.6967, 0.0001	6.4725, 6.4725, 0.0006

Part	PLA	Al
1	1.09	2.71
2	0.392	0.847
3	0.217	0.454
4	0.391	0.844

[5] "Quadrant - Global Manufacturer Of Engineering Plastics, High Performance Plastics, High Temperature Plastic Materials - Quadrant". *Quadrantplastics.com*. N.p., 2016. Web. 20 July. 2016.

GRAPH I

ROBOT TRAJECTORY
TEST
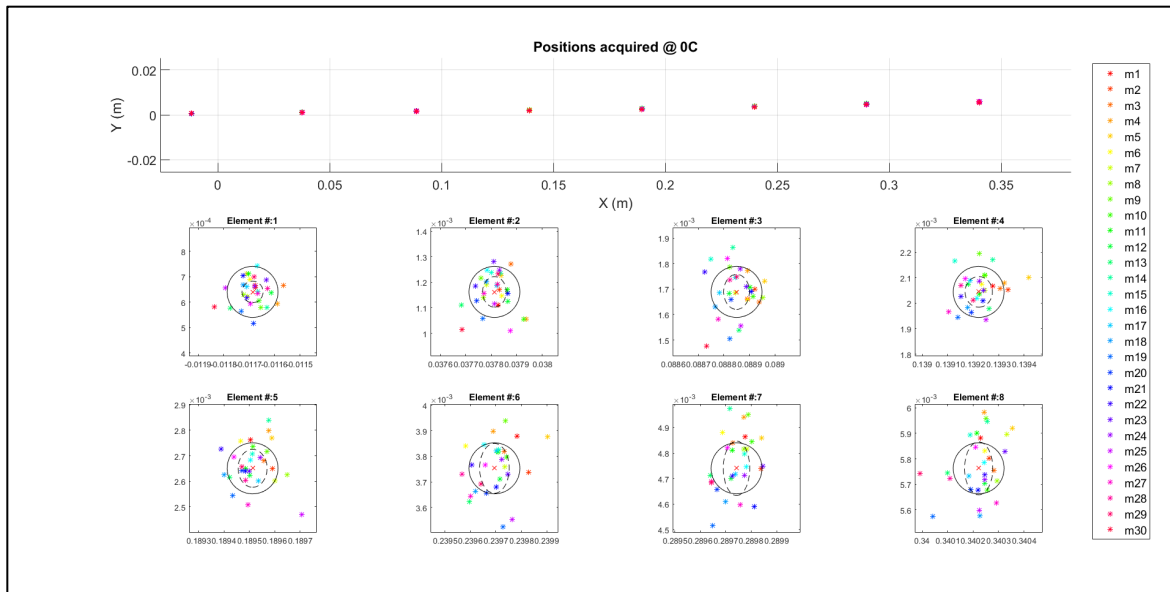
Graph I. Results of robot trajectory assessment. As the robot continues across the array, it becomes increasingly inaccurate, as illustrated by the increasing mean error.

ACKNOWLEDGMENTS

REFERENCES

[1] C. S. Wang, B. Y. Duan, F. S. Zhang and M. B. Zhu, "Coupled structural-electromagnetic-thermal modelling and analysis of active phased array antennas," in *IET Microwaves, Antennas & Propagation*, vol. 4, no. 2, pp. 247-257, Feb. 2010.

[2] Cheston Theodore and Joe Frank, "Phased array radar antennas." Radar Handbook. 1990

[3] D.S. Zrnic, J.F. Kimpel, D.E. Foryth, A. Shapiro, G. Crain, R. Ferek, J. Heimmer, W. Benner, T.J. McNellis, and R.J. Vogt, Agile-Beam Phased Array Radar For Weather Observations, *Bull. American Meteorological Society*, vol. 88, no. 11, pp. 1739-1751.

[4] National Severe Storms Laboratory, cited. 2006: New radar technology can increase tornado warning lead times. [Online http://www.norman.noaa.gov/publicaffairs/backgrounders/backgroun der_par.html].